Behavioral/Cognitive

Chemogenetic Disconnection between the Orbitofrontal Cortex and the Rostromedial Caudate Nucleus Disrupts Motivational Control of Goal-Directed Action

Kei Oyama,[1*] Yukiko Hori,[1*] Koki Mimura,[1*] Yuji Nagai,[1*] Mark A. G. Eldridge,[2] Richard C. Saunders,[2] Naohisa Miyakawa,[1] Toshiyuki Hirabayashi,[1] Yuki Hori,[1] Ken-ichi Inoue,[3] Tetsuya Suhara,[1] Masahiko Takada,[3] Makoto Higuchi,[1] Barry J. Richmond,[2] and Takafumi Minamimoto[1]

[1]Department of Functional Brain Imaging, National Institutes for Quantum Science and Technology, Chiba 263-8555, Japan, [2]Laboratory of Neuropsychology, National Institute of Mental Health, Bethesda, Maryland 20892, and [3]Center for the Evolutionary Origins of Human Behavior, Kyoto University, Inuyama 484-8506, Japan

The orbitofrontal cortex (OFC) and its major downstream target within the basal ganglia—the rostromedial caudate nucleus (rmCD)—are involved in reward-value processing and goal-directed behavior. However, a causal contribution of the pathway linking these two structures to goal-directed behavior has not been established. Using the chemogenetic technology of designer receptors exclusively activated by designer drugs with a crossed inactivation design, we functionally and reversibly disrupted interactions between the OFC and rmCD in two male macaque monkeys. We injected an adeno-associated virus vector expressing an inhibitory designer receptor, hM4Di, into the OFC and contralateral rmCD, the expression of which was visualized *in vivo* by positron emission tomography and confirmed by postmortem immunohistochemistry. Functional disconnection of the OFC and rmCD resulted in a significant and reproducible loss of sensitivity to the cued reward value for goal-directed action. This decreased sensitivity was most prominent when monkeys had accumulated a certain amount of reward. These results provide causal evidence that the interaction between the OFC and the rmCD is needed for motivational control of action on the basis of the relative reward value and internal drive. This finding extends the current understanding of the physiological basis of psychiatric disorders in which goal-directed behavior is affected, such as obsessive-compulsive disorder.

Key words: **DREADDs; monkey; motivation; PET; reward; striatum**

Significance Statement

In daily life, we routinely adjust the speed and accuracy of our actions on the basis of the value of expected reward. Abnormalities in these kinds of motivational adjustments might be related to behaviors seen in psychiatric disorders such as obsessive-compulsive disorder. In the current study, we show that the connection from the orbitofrontal cortex to the rostromedial caudate nucleus is essential for motivational control of action in monkeys. This finding expands our knowledge about how the primate brain controls motivation and behavior and provides a particular insight into disorders like obsessive-compulsive disorder in which altered connectivity between the orbitofrontal cortex and the striatum has been implicated.

Received Jan. 30, 2022; revised Apr. 20, 2022; accepted June 5, 2022.

Author contributions: T.M. designed research; K.O., Y.H., K.M., Y.N., M.A.G.E., R.C.S., N.M., K.I., and T.M. performed research; Y.H., K.M., Y.N., Y.H., and T.M. analyzed data; K.O., Y.H., K.M., Y.N., M.A.G.E., R.C.S., N.M., T.H., Y.H., K.-i.,I., T.S., M.T., M.H., B.J.R., and T.M. wrote the paper.

This work was supported by the Japan Society for the Promotion of Science Grants JP21K07268 (K.O.) and JP15H05917, JP15K21742, and JP20H05955 (T.M.); Japan Agency for Medical Research and Development Grants JP18dm0307007 (T.H.), JP19dm0207077 (M.T.), and JP16dm0107146 (T.M.); Intramural Research Program of the National Institute of Mental Health Grant ZIAMH002619; Cooperative Research Program (Grant 2021-A-14) at the Primate Research Institute, Kyoto University; and the National BioResource Project, Japanese Monkeys, of the Ministry of Education, Culture, Sports, Science, and Technology, Japan. We thank Jun Kamei, Ryuji Yamaguchi, Yuichi Matsuda, Yoshio Sugii, Takashi Okauchi, Tomomi Kokufuta for technical assistance.

*K.O., Y.H., K.M., and Y.N. contributed equally to this work.

The authors declare no competing financial interests.

Correspondence should be addressed to Takafumi Minamimoto at minamimoto.takafumi@qst.go.jp.

https://doi.org/10.1523/JNEUROSCI.0229-22.2022

Copyright © 2022 Oyama et al.

This is an open-access article distributed under the terms of the Creative Commons Attribution 4.0 International license, which permits unrestricted use, distribution and reproduction in any medium provided that the original work is properly attributed.

Introduction

The subjective desirability (i.e., value) of an expected reward is a key factor in determining the latency, accuracy, and vigor of goal-directed behavior (Dickinson and Balleine, 1994). Goal-directed behavior is regulated by two factors, the incentive value of the goal (reward) and the internal drive (physiological state) of an agent (Berridge, 2004; Zhang et al., 2009). The orbitofrontal cortex (OFC) is thought to be critical for the ability of an animal to adjust behavior based on reward value. Neuronal activity in the OFC is substantially modulated by the sensory and hedonic properties of rewards (Rolls et al., 1989; de Araujo and Rolls, 2004) as well as subjective reward preference (Padoa-Schioppa and Assad, 2006; Chaudhry et al., 2009). Inactivation or lesion of the bilateral OFC disrupts the ability to use stimulus information for directing behaviors to optimize the outcome (Izquierdo et al., 2004; Murray et al., 2015). However, it remains unclear which downstream region receives the value-related information from the OFC and processes it for implementing goal-directed behavior.

Although the ventral part of the striatum is generally regarded as the primary basal ganglia destination downstream of the OFC, anatomic studies in monkeys have reported that the rostromedial part of the caudate nucleus (rmCD) also receives direct ipsilateral connections from the OFC, specifically Brodmann areas (BA)11 and BA13 (Haber et al., 2006). Electrophysiological recording studies in monkeys have reported that neuronal activity in the rmCD signals information about the expected reward value and satiation level but exhibits a relatively weak selectivity for movements (Hollerman et al., 1998; Nakamura et al., 2012; Fujimoto et al., 2019). Additionally, temporary inactivation of bilateral, but not unilateral, rmCD neuron activity impaired the ability of monkeys to adjust their motivation based on incentive cues (Nagai et al., 2016). Moreover, research in rodents has demonstrated that the projection from the OFC to the dorsomedial striatum is a critical pathway for carrying the incentive information and behaving in a goal-directed manner (Yin et al., 2005; Gremel and Costa, 2013; Gremel et al., 2016). These findings thus provide a plausible scenario in which the primate OFC–rmCD projection contributes to the motivational adjustment of action based on incentive and drive; however, this has not yet been directly examined. Addressing this issue is particularly important considering that disrupted functional connectivity between the OFC and the striatum is implicated in many human psychiatric disorders, including obsessive-compulsive disorder (OCD), whose symptoms seem to be associated with impaired motivational control of behavior (Harrison et al., 2009; Figee et al., 2013; Abe et al., 2015; Jahanshahi et al., 2015; Gillan et al., 2016).

To determine the contribution of the OFC–rmCD pathway in goal-directed behavior, here we used a chemogenetic technology, designer receptors exclusively activated by designer drugs (DREADDs), with a crossed inactivation design to reversibly disrupt their direct intrahemispheric information flow. We virally introduced an inhibitory designer receptor (hM4Di) into OFC and contralateral rmCD neurons in two macaque monkeys. We used a reward-size task to examine the effect of temporarily disconnecting these areas on the ability of the monkeys to adjust goal-directed actions based on motivation. The relationships between motivational value, incentive, and drive were inferred from task performance. We show that following systemic administration of DREADD agonists, goal-directed behavior in monkeys was altered so that they became insensitive to differences in reward magnitude and satiation.

Materials and Methods

Animals. Two male macaque monkeys participated in the experiments, MK#1, rhesus monkey (*Macaca mulatta*), 7.3 kg, age 10.3 years at the start of experiments and MK#2, Japanese monkey (*Macaca fuscata*), 6.1 kg, age 4.4 years at the start of experiments. All experimental procedures involving animals were conducted in accordance with the *Guide for the Care and Use of Nonhuman Primates in Neuroscience Research* (Japan Neuroscience Society; https://www.jnss.org/en/animal_primates) and were approved by the Animal Ethics Committee of the National Institutes for Quantum Science and Technology. A standard diet, supplementary fruits/vegetables, and a tablet of vitamin C (200 mg) were provided daily.

Viral vector production. Adeno-associated virus 2 (AAV2) vectors (AAV2-CMV-hM4Di and AAV2-CMV-AcGFP) were produced by helper-free triple transfection and purified by affinity chromatography (GE Healthcare). Viral titer was determined by quantitative PCR using TaqMan technology (Life Technologies).

Surgical procedures and viral vector injections. Surgeries were performed under aseptic conditions in a fully equipped operating suite. We monitored body temperature, heart rate, SpO_2, and tidal CO_2 throughout all surgical procedures. Anesthesia was induced using an intramuscular injection of ketamine (5–10 mg/kg) and xylazine (0.2–0.5 mg/kg), and monkeys were intubated with an endotracheal tube. Anesthesia was maintained with isoflurane (1–3%, to effect). After surgery, prophylactic antibiotics and analgesics were administered. Before surgery, magnetic resonance imaging (MRI; 7 Tesla 400 mm/SS system, NIRS/KOBELCO/Brucker) and x-ray computed tomography (CT) scans (Accuitomo 170, MORITA) were acquired under anesthesia (continuous infusion of propofol 0.2–0.6 mg/kg/min, intravenously). Overlaid MR and CT images were created using PMOD image analysis software (PMOD Technologies) to estimate stereotaxic coordinates of target brain structures.

The monkeys were first co-injected with AAV2-CMV-hM4Di (1.0 × 1013 and 2.3 × 1013 particles/ml, respectively) and AAV2-CMV-AcGFP (4.7 × 1012 and 6.6 × 1012 particles/ml, respectively) into the OFC of one hemisphere (BA11 and BA13; right and left hemispheres, respectively; Fig. 1*B*,*C*). The injections were performed under direct vision. The OFC was visualized using the same types of surgical procedures as used as a previous study (Eldridge et al., 2016). Briefly, after retracting skin, galea, and muscle, the frontal cortex was exposed by removing a bone flap and reflecting the dura mater. Handheld injections were then made under visual guidance through an operating microscope (Leica M220, Leica Microsystems), with care taken to place the beveled tip of a microsyringe (model 1701RN, Hamilton) containing the viral vector at an angle oblique to the brain surface. The needle (26 gauge, point style 2) was inserted into the intended area of injection by one experimenter, and a second experimenter pressed the plunger to expel ~1 μl per penetration. Totals of 54 μl and 50 μl were injected for MK#1 and MK#2 via 53 and 49 tracks, respectively.

At 174 and 196 d after the first injection, the monkeys received a second set of injections with the same vectors into the rmCD contralateral to the OFC injections (Fig. 1*B*,*C*) using a procedure used in a previous study (Nagai et al., 2016). Briefly, viruses (total volume, 3 μl for both monkeys) were pressure injected by a 10 μl microsyringe (model 1701RN, Hamilton) with a 30 gauge injection needle in a fused silica capillary (450 mm outer diameter) to create a step ~500 μm away from the needle tip to minimize backflow. The microsyringe was mounted into a motorized microinjector (catalog #UMP3T-2, World Precision Instruments) that was held by a manipulator (model 1460, David Kopf) on the stereotaxic frame. After a burr hole (8 mm diameter) and the dura mater (~5 mm) were opened, the injection needle was inserted into the brain and slowly moved down 2–3 mm beyond the target, then kept stationary for 5 min, after which it was pulled up to the target location. The injection speed was set at 0.5 μl/min. After the injection, the needle remained *in situ* for 15 min to minimize backflow along the needle.

Behavioral task. Before the experiments, monkeys were trained for >3 months to discriminate the color of shapes presented on a computer monitor. For the experiment, we used a reward-size task, as described

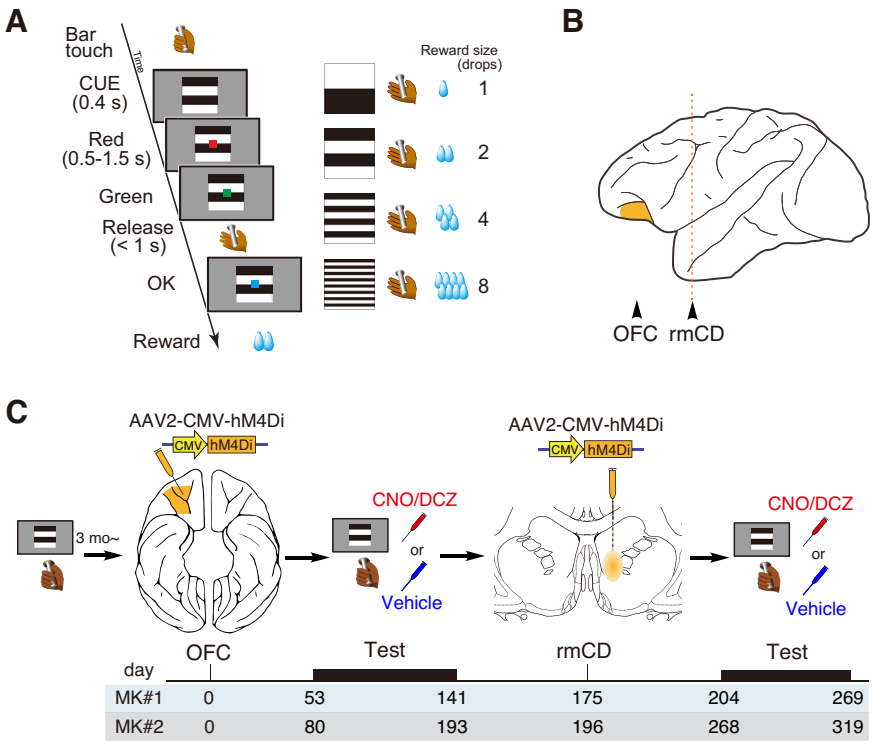

Figure 1. Task and experimental design. ***A***, The reward-size task. Left, At the beginning of each trial, a visual cue signaled the amount of reward (1, 2, 4, or 8 drops) that would be delivered after a correct red/green color discrimination. After each correct trial, a new cue reward-size pair was picked from the set of four at random. Right, Relationship between cues and reward sizes. ***B***, Lateral view of monkey brain. Locations of the OFC and rmCD are indicated by arrowheads. ***C***, Experimental design and timeline. The monkeys were first trained on the reward-size task, followed by injections of the hM4Di vector into the OFC (orange) to produce unilateral OFC silencing when DREADD agonists were administered. Another AAV vector was then injected into the contralateral rmCD to enable functional disconnection of the OFC–rmCD pathway when the DREADD agonists were administered. Bottom, Numbers indicate the days after OFC injection.

previously (Minamimoto et al., 2009; Fig. 1*A*), which followed a cued multitrial reward schedule. Task control and data acquisition were performed using a QNX-based Real-time EXperimentation data acquisition system (REX; Laboratory of Sensorimotor Research, National Eye Institute) and commercially available software (Presentation, NeuroBehavioral System). The use of an automated system eliminated the need for experimenters to be blind to treatment. A monkey initiated a trial by touching a bar. A background visual cue and a red target appeared sequentially on the display. After a variable interval, the red target turned green. If the monkey released the bar between 200 and 1000 ms after this event, the target turned blue, and a liquid reward (one, two, four, or eight drops; one drop equal to ~ 0.1 ml) was delivered immediately afterward. If the monkey released the bar outside the 200–1000 ms range, we regarded the trial as an error trial, which was aborted and repeated after a 1000 ms intertrial interval. The visual cue presented at the beginning of the trial indicated the amount of reward that would be received if the trial was completed successfully. After an error, the monkey had to repeat the same trial condition and correctly complete it to receive a reward. Because the monkeys were able to perform the task correctly on nearly every trial when the visual cues did not convey the information about the amount of reward, error trials were interpreted as those in which the monkeys were not sufficiently motivated to release the bar correctly (Minamimoto et al., 2009). Our behavioral measure for the expected outcome value was the proportion of error trials (i.e., error rates). Before each 100 min testing session, the monkeys went without water for ~22 h. Both monkeys were trained on the reward-size task for at least 3 weeks before the experiments.

Drug administration. We used clozapine N-oxide (CNO) and deschloroclozapine (DCZ) as DREADD actuators for MK#1 and MK#2, respectively. CNO (Toronto Research) and DCZ (MedChemExpress) were dissolved in 2.0% or 2.5% dimethylsulfoxide (DMSO, FUJIFILM Wako Pure Chemical). These stock solutions were diluted in saline to a final volume of 2 ml at a dose of 3 mg/kg (CNO) or 1 ml at a dose of 0.03 mg/kg (DCZ) and injected intravenously or intramuscularly 15 min before the beginning of the experiments, respectively. These doses of CNO or DCZ yield 50–60% hM4Di occupancy but do not affect the performance of monkeys that are not expressing hM4Di (Nagai et al., 2016, 2020). CNO/DCZ and vehicle treatment were tested no more than once per week.

Positron emission tomography imaging. To examine the expression of hM4Di *in vivo*, positron emission tomography (PET) imaging was conducted before vector injection and ~8 weeks after injection for MK#2, as previously reported (Nagai et al., 2016, 2020). Briefly, the monkey was anesthetized with ketamine (5–10 mg/kg, i.m.) and xylazine (0.2–0.5 mg/kg, i.m.), which was maintained with isoflurane (1%–3%) during all PET procedures. PET scans were performed using a microPET Focus 220 scanner (Siemens Medical Solutions). Transmission scans were performed for ~20 min with a ^{68}Ge source. Emission scans were acquired in 3D list mode with an energy window of 350–750 keV after an intravenous bolus injection of [^{11}C]DCZ (324.5–384.9 MBq). Emission-data acquisition lasted 90 min. PET image reconstruction was performed with filtered back projection using a Hanning filter cutoff at a Nyquist frequency of 0.5 mm^{-1}. To estimate the specific binding of [^{11}C]DCZ, the regional binding potential relative to nondisplaceable radioligand (BP_{ND}) was calculated using PMOD with an original multilinear reference tissue model (MRTMo) and the cerebellum as a reference (Nagai et al., 2016; Yan et al., 2021). Contrast (subtraction) images were constructed using SPM12 software (Wellcome Center for Human Neuroimaging; https://www.fil.ion.ucl.ac.uk) and MATLAB R2016a software (MathWorks). The surface of the gray matter was estimated on the basis of the MR image. Briefly, Yerkes standard T1 and T2 templates (Donahue et al., 2016, 2018) were first linearly and nonlinearly registered to the original MR image using the Functional MRI of the Brain (FMRIB) linear registration tool (FLIRT) and the FMRIB nonlinear registration tool (FNIRT) in the FMRIB Software Library software (Smith et al., 2004). The gray matter surface was then estimated using registered templates and the Human Connectome Project–Nonhuman Primates structural pipeline (Autio et al., 2020). Finally, a contrast PET image was projected on the gray matter surface using Connectome Workbench software (https://www.humanconnectome.org/software/get-connectome-workbench), followed by registration of the contrast PET image to the original MR image.

Histology and immunostaining. For histologic inspection, two monkeys were deeply anesthetized with an overdose of sodium pentobarbital (80 mg/kg, i.v.) and transcardially perfused with saline at 4°C, followed by 4% paraformaldehyde in 0.1 M PBS, pH 7.4. The brain was removed from the skull, postfixed in the same fresh fixative overnight, saturated with 30% sucrose in phosphate buffer at 4°C, then cut serially into 50-μm-thick sections on a freezing microtome. For visualization of immunoreactive signals of GFP coexpressed with hM4Di, every sixth section was immersed in 1% skim milk for 1 h at room temperature and incubated overnight at 4°C with rabbit anti-GFP monoclonal antibody (1:200–500; catalog #G10362, Thermo Fisher Scientific), then for 2 d in PBS containing 0.1% Triton X-100 and 1% normal goat serum at 4°C. The sections were then incubated in the same fresh medium containing biotinylated goat anti-rabbit IgG antibody (1:1000; Jackson ImmunoResearch) for 2 h at room

temperature, followed by avidin-biotin-peroxidase complex (ABC Elite, Vector Laboratories) for 2 h at room temperature. For visualization of the antigen, the sections were reacted in 0.05 M Tris-HCl buffer, pH 7.6, containing 0.04% diaminobenzidine (DAB), 0.04% $NiCl_2$, and 0.003% H_2O_2. The sections were then mounted on gelatin-coated glass slides, air dried, and coverslipped. A second series of sections was Nissl stained with 1% cresyl violet. Images of sections were digitally captured using an optical microscope equipped with a high-grade charge-coupled device camera (BZ-X710, Keyence) or a whole slide scanner (NanoZoomer S60, Hamamatsu Photonics).

Experimental design and statistical analysis . For behavioral data analysis, the error rate for each reward size was calculated for each daily session. We used the error rates to estimate the level of motivation as the error rates of these tasks (E) were inversely related to the value for action. In the reward-size task, we used an inverse function as follows:

$$E = \frac{c}{R + b}, \tag{1}$$

where E is error rate, R is reward size, and c and b are constants.

To examine the effects of satiation, we divided each session into quartiles based on normalized cumulative reward, R_{cum}, which was 0.125, 0.375, 0.625, and 0.875 for the first through fourth quartiles, respectively. We fitted the error rates obtained from each monkey to the following model:

$$E = \frac{c}{(R + b) \times F(R_{cum})}, \tag{2}$$

where the satiation effect, $F(R_{cum})$, represents the exponentially decaying reward value (at a constant rate) as reward accumulates (i.e., R_{cum} increases; Minamimoto et al., 2012) as follows:

$$F(R_{cum}) = e^{-\lambda R_{cum}}. \tag{3}$$

We fitted the functions to the data using sum-of-squares minimization. We performed repeated-measures ANOVA with individual monkeys nested to test the effect of treatment and its interactive effect with reward size and satiation on error rates. For example, the effect of treatment × reward size on error rates was examined using an R code, aov(error ~ treatment * reward + Error[subject], data). Separate ANOVAs were also conducted on data of each subject for confirmation.

Results

Unilateral silencing of the OFC had little effect on reward-size task performance

Both monkeys were injected with AAV vectors expressing hM4Di in unilateral OFC (BA11 and BA13; Fig. 1*C*). Eight weeks after the injection, we visualized the expression of the DREADD *in vivo* via PET imaging using the DREADD-selective radioligand ^{11}C-labeled DCZ (Nagai et al., 2020). As shown in Figure 2, *A* and *B*, an increase in PET signal covered the target region of the OFC, which indicated hM4Di expression. Expression in individual OFC neurons was verified using postmortem immunohistochemical staining for the coexpressed *Aequorea coerulescens* (Ac)GFP (Fig. 2*C*), at an anteroposterior level corresponding to Figure 2, *A*, A1–A3, and *B*, A1–A3, in both monkeys.

To examine the ability to estimate reward and adjust behavior, we tested the monkeys on the reward-size task (Fig. 1*A*). The task requirement (i.e., release the bar on time) was so simple that after 3 months of training, the monkeys could complete high incentive trials with a near 100% rate of accuracy if sufficiently motivated (Minamimoto et al., 2009). Errors (either releasing the bar too early or too late) were typically observed in small reward

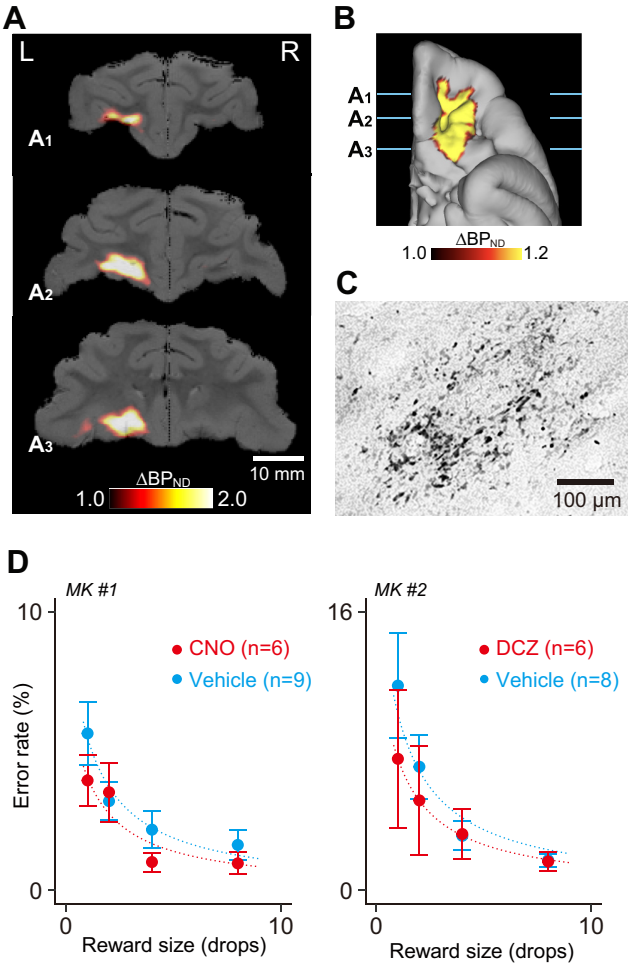

Figure 2. Effect of unilateral chemogenetic OFC inactivation on reward evaluation. ***A***, ***B***, *In vivo* visualization of hM4Di in the OFC using PET. Coronal parametric image (A1–A3, anterior to posterior) and ventral view of flat map (***B***) showing increased tracer [^{11}C]DCZ binding (BP_{ND}) 58 d after hM4Di vector injection compared with prevector injection, overlaid on the MR image for MK#2. ***C***, Bright-field image of a coronal DAB-stained section showing GFP-positive neurons in the OFC. ***D***, Effect of chemogenetic silencing of unilateral OFC on performance during the reward-size task in MK#1 (left) and MK#2 (right), respectively. Error rates as a function of reward size (mean ± SEM) are plotted for DREADD agonist (red) and vehicle (cyan) treatment conditions. Curves are the best fit function of Equation 1. We found no significant effect of silencing on error rates in either monkey (MK#1, $F_{(1,52)} = 1.9$, $p = 0.17$; MK#2, $F_{(1,48)} = 0.98$, $p = 0.33$).

trials and/or close to the end of daily sessions and were therefore considered as a behavioral indicator that the monkeys were not sufficiently motivated to correctly release the bar. As shown in earlier studies (Minamimoto et al., 2009), the error rates were related to the value of the upcoming reward (Fig. 2*D*), with fewer errors occurring when expected reward was high. Overall error rates after treatment with the DREADD agonists CNO or DCZ did not differ from those after injection with vehicle control (two-way ANOVA, main effect of treatment, $F_{(1,107)} = 2.1$, $p = 0.16$; Fig. 2*D*). We consistently observed a significant effect of reward on error rates (main effect of reward size, $F_{(3,107)} = 10.9$, $p = 2.7 \times 10^{-6}$) but not of the interaction (reward × treatment, $F_{(3,107)} = 0.49$, $p = 0.69$). This result suggests that unilateral silencing of the OFC did not interfere with the normal ability to estimate reward, which is in accordance with a previous study of OFC lesions (Clark et al., 2013).

Unilateral OFC inactivation did not alter the frequency of error types (early or late errors; two-way ANOVA, main effect of

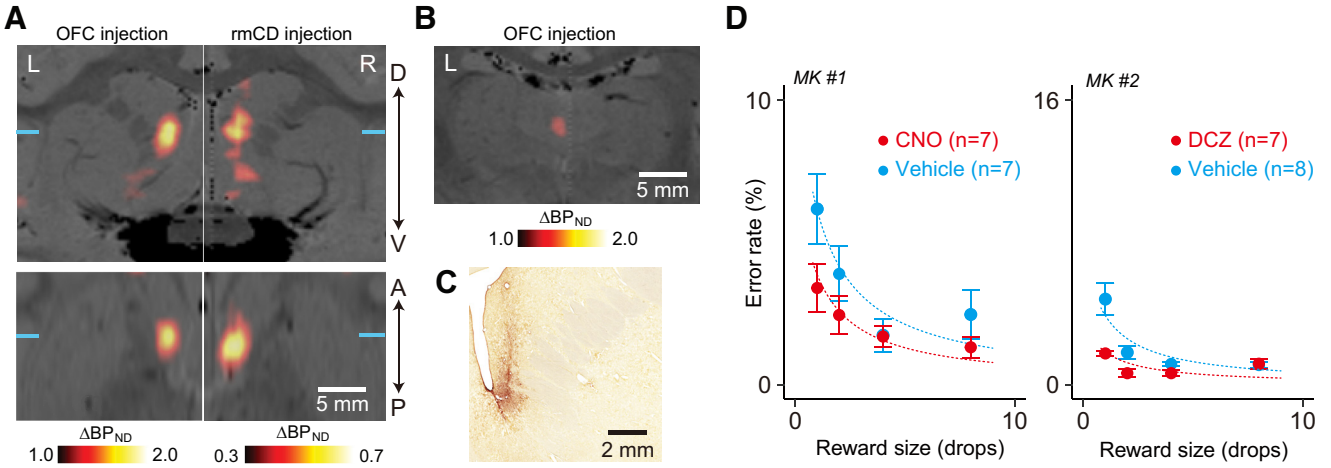

Figure 3. Chemogenetic disconnection of OFC–rmCD reduced the sensitivity to reward amount. ***A***, *In vivo* visualization of hM4Di in the rmCD using PET. Coronal (top) and horizontal PET images (bottom) representing increased relative tracer binding (BP_{ND}) 58 d after vector injection into the OFC (OFC injection, left) and 57 d after injection into the rmCD (rmCD injection, right) compared with prevector injection, overlaid on an MR image for MK#2. L, Left, R, right. Each coronal and horizontal section was acquired at the anteroposterior (A–P) and dorsoventral (D–V) levels indicated by corresponding blue lines, respectively. ***B***, Coronal PET image representing increased BP_{ND} in the mediodorsal thalamus, indicating hM4Di-positive OFC axon terminals. ***C***, Bright-field image of a coronal DAB-stained section showing immunoreactivity against a reporter protein (GFP) in the rmCD for MK#2. ***D***, Effect of chemogenetic functional disconnection of the OFC and rmCD on performance during the reward-size task in MK#1 (left) and MK#2 (right), respectively. Error rates as a function of reward size (mean ± SEM) are plotted for DREADD agonist (red) and vehicle (cyan) treatment conditions. Curves are the best fit function of Equation 1. A significant main effect of treatment was observed in both monkeys (MK#1, $F_{(1,48)} = 6.0$, $p = 0.018$; MK#2, $F_{(1,52)} = 17.1$, $p = 1.3 \times 10^{-4}$).

treatment, $F_{(1,26)} = 1.5$, $p = 0.24$). The treatment significantly shortened reaction time (two-way ANOVA; treatment, $F_{(1,107)} = 43.1$, $p = 1.9 \times 10^{-9}$). Reward size also had significant impact on reaction time ($F_{(3,107)} = 9.2$, $p = 1.9 \times 10^{-5}$) but without significant interaction with treatment (reward × treatment: $F_{(3,107)} = 0.08$, $p = 0.97$). Total reward earned significantly increased following inactivation ($F_{(1,26)} = 6.0$, $p = 0.02$). However, no significant interaction was observed between treatment and satiation on error rates (three-way ANOVA with treatment, reward size, and satiation; treatment × satiation, $F_{(3,31)} = 0.81$, $p = 0.50$; see below, Discussion).

Chemogenetic disconnection of OFC–rmCD reduced the sensitivity to the amount of expected reward

Next, we examined the causative role of the functional connection between the OFC and the rmCD by contralateral (crossed) inactivation of these two areas. After OFC vector injection, PET showed increased binding of [^{11}C]DCZ in the ipsilateral rmCD (Fig. 3*A*, left), reflecting hM4Di-positive axon terminals (i.e., anatomic connection from the OFC to the rmCD as reported in previous anatomic studies; Haber et al., 2006). Increased binding of [^{11}C]DCZ was also found in the ipsilateral medial part of the mediodorsal thalamus (Fig. 3*B*). We then injected the viral vector into the rmCD contralateral to the first injections (Fig. 1*C*). The [^{11}C]DCZ-PET scans detected the expression of hM4Di in the rmCD as increased tracer binding extending 2–3 mm anterior to posterior, resulting in a mirror image of the OFC terminal site (Fig. 3*A*). This was further verified by postmortem immunohistochemical staining for the coexpressed AcGFP for both monkeys (Fig. 3*C*).

We then tested the monkeys on the reward-size task following treatment with the DREADD agonists or vehicle control. We found that error rates were consistently lower after treatment with the DREADD agonists compared with those after treatment with vehicle controls (Fig. 3*D*; two-way ANOVA, main effect of treatment, $F_{(1,107)} = 17.7$, $p = 5.4 \times 10^{-5}$). The treatment had a significant interaction effect with reward size (reward × treatment, $F_{(3,107)} = 3.9$, $p = 0.011$) so that treatment reduced error rates more for trials in which expected rewards should have been small, whereas the impact of reward on error rates remained significant (main effect of reward size, $F_{(3,107)} = 17.7$, $p = 2.1 \times 10^{-9}$). Considering that the unilateral inactivation of either OFC (Fig. 2*D*) or rmCD alone (Nagai et al., 2016) did not change error rates on this task, our results suggest that functional disconnection between OFC and rmCD reduced the sensitivity to differences in reward size.

We further examined the effect of the OFC–rmCD chemogenetic disconnection on other behavioral parameters. We found that disconnection significantly increased the early/late error ratio (main effect of treatment, $F_{(1,26)} = 11.2$, $p = 0.0025$). The disconnection tended to shorten reaction time (two-way ANOVA; main effect of treatment, $F_{(1,107)} = 3.9$, $p = 0.051$), whereas the impact of reward remained significant (main effect of reward size, $F_{(3,107)} = 3.8$, $p = 0.012$). The treatment had no significant interactive effect with reward size on reaction time (treatment × reward size, $F_{(3,107)} = 0.6$, $p = 0.60$).

Chemogenetic disconnection of OFC–rmCD reduced the impact of satiation on performance

The motivational value of reward should decrease as the physiological drive state changes from thirst to satiation. Because it has been shown that this devaluation effect on goal-directed action is vdiminished after OFC lesions (Izquierdo et al., 2004), the decreased sensitivity to reward magnitude that we observed might have resulted from decreased sensitivity to satiation shift. In all daily sessions, the monkeys were allowed to keep performing the task until they did not want to anymore, meaning that the final data each day were collected as the monkeys were approaching satiation. When treated with the vehicle, overall error rates for each reward size increased as the normalized cumulative reward (R_{cum}) increased (Fig. 4, left). In contrast, satiation-dependent changes in error rates were not pronounced following treatment with the DREADD agonists (Fig. 4, right). Indeed, we observed a significant interaction between treatment

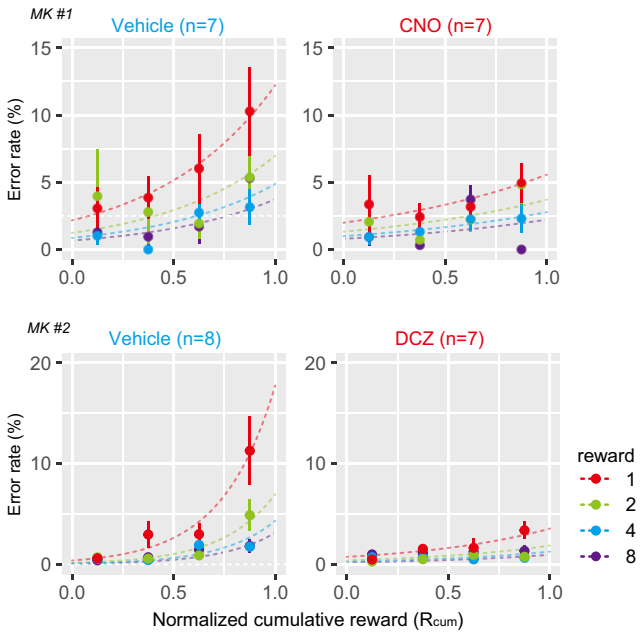

Figure 4. Chemogenetic disconnection of OFC–rmCD reduced the impact of satiation on performance. Error rates as a function of normalized cumulative reward (mean ± SEM) are plotted for vehicle (left) and DREADD agonist treatment conditions (right) in MK#1 (top) and MK#2 (bottom), respectively. Reward condition (amount) is color coded. Curves are the best fit function of Equation 2.

and satiation on error rates (three-way ANOVA with treatment, reward size, and satiation; treatment × satiation, $F_{(3,31)} = 9.06$, $p = 1.9 \times 10^{-4}$). As OFC–rmCD disconnection did not change the amount of total reward received ($F_{(1,26)} = 2.18$, $p = 0.15$), the drive for water or general motivation to perform the task did not seem to have been altered. Collectively, these data suggest that OFC–rmCD disconnection significantly attenuated the impact of satiation on goal-directed performance.

Discussion

To examine the causal role of the communication through the OFC–rmCD pathway in goal-directed behavior, we used DREADD technology to functionally and temporarily disconnect these brain areas in two macaques. Activation of hM4Di in the OFC and the contralateral rmCD produced a significant and reproducible loss of normal sensitivity to the cued reward value for goal-directed action. The disconnection did not decrease general attention or drive, as evidenced by the unaffected reaction times and the total amount of reward earned. Reduced sensitivity to reward size was most prominent when monkeys had accumulated a certain amount of reward, suggesting that the satiation effect on motivation depends on the integrity of the OFC–rmCD connections.

Expectation of the reward value is the hallmark of motivational control of behavior. The motivational value comprises both external incentives and internal drives. In the reward-size task, visual cues always indicated the amount of reward for a given trial. At the same time, the motivation to receive the reward—indexed by bar-releasing error rates—became less as the monkeys drank throughout the session. Thus, the motivational value of the cue was dynamically updated according to the degree of satiation. Previous studies using the reward-size task have shown that the OFC and rmCD control normal estimates of the cued outcome value. Specifically, monkeys with OFC ablation performed this task with smaller differences in error rates, suggesting less sensitivity to relative reward amount (Simmons et al., 2010). When the rmCD was inactivated bilaterally, by using DREADDs or muscimol, the overall error rates increased, and their discrimination of reward sizes diminished, indicating the decreased sensitivity to absolute and relative value estimation, respectively (Nagai et al., 2016). In these cases, however, the impact of satiation on performance remained normal. In contrast to these previous studies, the present work demonstrated that the OFC–rmCD disconnection reduced the impact of reward magnitude and satiation and resulted in seemingly higher motivation when the reward value became small. In the same monkeys, however, the impact of incentive or satiation was unchanged when the unilateral OFC alone was silenced. Although the current study did not compare the behavioral effects of two silencing conditions directly, our results, together with the nonsignificant effects of unilateral rmCD silencing (Nagai et al., 2016), support the notion that the effects of OFC–rmCD disconnection is not the sum of two unilateral effects. Thus, our findings extend those of previous reports in an important way, indicating that communication from the OFC to the rmCD is critical for value updating and/or adjusting behavior based on internal drive.

Neurons in the OFC are known to represent the values of reward-predicting stimuli (Roesch and Olson, 2004; Padoa-Schioppa and Assad, 2006; Bouret and Richmond, 2010; Kobayashi et al., 2010; Hosokawa et al., 2013; Rudebeck et al., 2013b; Rich and Wallis, 2016; Yun et al., 2020). Neurons in the rmCD are also known to signal incentive values of future action (Nakamura et al., 2012; Fujimoto et al., 2019). Moreover, neuronal signals in both the OFC and the rmCD have been shown to be affected by the internal states of satiety. For example, reward-specific satiety reduced OFC neuronal signals related to olfactory and gustatory stimuli (Rolls et al., 1989; Critchley and Rolls, 1996) and the subjective value for economic choice (Pastor-Bernier et al., 2021). Additionally, task-related activity of some rmCD neurons was modulated by the satiation level in the reward-size task (Fujimoto et al., 2019). However, the loss of these value- and satiety-related neuronal signals by lesions or inactivation at each stage did not affect the satiation effect on goal-directed action, as discussed above. Thus, the behavioral alterations observed in the monkeys following the OFC–rmCD disconnection in our study may have been caused by the loss of interaction of these neuronal signals through this connection.

Lesions of the OFC have been repeatedly shown to abolish normal choice adapting behavior to changes in reward value through satiety (i.e., devaluation effect; Izquierdo et al., 2004; Machado and Bachevalier, 2007; Baxter et al., 2009; Rudebeck et al., 2013a). Furthermore, inactivation studies revealed that the OFC (i.e., BA13) is essential for updating the valuation of expected reward outcomes, whereas BA11 is critical for translating this knowledge into goals (West et al., 2011; Murray et al., 2015). Several studies in rodents have also reported that satiation-induced decreases in instrumental actions were blocked by inactivation of the projection from the OFC to the dorsomedial striatum (Yin et al., 2005; Gremel and Costa, 2013; Gremel et al., 2016). Our data are consistent with these previous findings and highlight the role of the primate OFC–rmCD pathway in the motivational adjustment of action on the basis of incentive and drive.

Inactivation of the unilateral OFC significantly shortened the reaction time and increased the total reward accumulation, which may suggest a general increase in motivation. These effects

were not lateralized as they were observed in both monkeys, although the silenced OFCs were in opposite hemispheres. Such phenomena are not similar to the deficits that we observed following OFC–rmCD disconnection—an impairment in motivational control of goal-directed action. Although the exact contribution of the OFC in one hemisphere to motivational control of behavior remains an open question, our results indicate that the specific functional connection between the OFC and the rmCD is critical for modulating behavior on the basis of the expected reward value.

In the present study, functional disconnection was attempted by expressing inhibitory DREADDs in the OFC and rmCD contralaterally, as in a crossed-lesion disconnection design (Baxter et al., 2000; Clark et al., 2013; Eldridge et al., 2016). Because the expression of hM4Di in the rmCD mirrored that in the terminal field of OFC–rmCD projection (compare Fig. 3*A*), the crossed chemogenetic silencing appeared to disrupt the communication between the OFC and the rmCD bilaterally. However, for anatomic disconnection, a pathway-specific chemogenetic silencing method would be ideal, such as local agonist delivery (Oyama et al., 2021) or a double viral vector system (Oguchi et al., 2021). It should also be noted here that the two DREADD actuators, CNO and DCZ, were used in our study. This was because DCZ was developed in parallel with the progress of the present experiment. Regardless of the actuator used, comparable and consistent behavioral changes specifically occurred after completion of bilateral vector injections, confirming that this event was caused by the hM4Di-mediated functional disconnection between the OFC and the rmCD, rather than other factors such as off-target actions of metabolites.

The current findings do not exclude the possibility that the impairment observed following OFC–rmCD disconnection is caused by removing motivational processing at a third structure receiving input from OFC and rmCD. For example, the medial magnocellular part of the mediodorsal thalamus (MDmc) is known to receive input directly from the OFC (McFarland and Haber, 2002; Xiao et al., 2009) and from rmCD via the ventral pallidum (Russchen et al., 1987). Indeed, our PET data indicated the presence of hM4Di-positive terminals in the MDmc (Fig. 3*B*). Furthermore, lesions of the MDmc have been reported to disrupt reinforcer devaluation effects in monkeys (Mitchell et al., 2007). Thus, further studies are needed to identify the pathways that contribute to OFC and rmCD communication in goal-directed behavior.

Our findings further have important implications for understanding neuropsychiatric disorders, whose symptoms can be associated with abnormal motivational control of behavior. For example, patients with OCD show a general impairment in the ability to flexibly adjust their behaviors to changes in outcome values, resulting in an over-reliance on habits (Gillan et al., 2011; Gillan and Robbins, 2014). Deficits in goal-directed control are also observed in other conditions, including major depressive disorders, substance abuse, and binge-eating disorders (Griffiths et al., 2014; Jahanshahi et al., 2015; Fettes et al., 2017). Neuroimaging studies have suggested dysfunction of the prefronto-striatal network in the pathophysiology of these disorders (Figee et al., 2013; Abe et al., 2015; Foerde et al., 2015; Voon et al., 2015; Ng et al., 2019; Sha et al., 2020). In this context, the present study provides valuable causal information about a specific neural network in primates. Future chemogenetic studies combined with functional MRI will provide a unique opportunity to link behavioral and network changes in monkeys (Hirabayashi et al., 2021) and directly compare these changes with those seen in human psychiatric disorders. As a component of this future research, it would be useful to assess obsessive-compulsive or other behaviors that are not addressed in the current study.

In summary, chemogenetic disconnection of communication between the OFC and the rmCD produced a significant impairment in the normal estimate of reward value along with satiation. Our observations are in accordance with previous evidence for neuronal signaling related to incentive and drive that has been identified in these structures during goal-directed behavior. Additionally, previous lesion and inactivation studies of these brain areas suggest a causal role of value signals related to the OFC and the rmCD in behavioral adjustment. Our results extend these previous findings and directly demonstrate that the functional connection between the OFC and the rmCD is critical for generating motivational value based on the integration of external stimuli with internal drive in monkeys. The present data also have clinical implications that could be useful for advancing our understanding of the pathophysiology of certain psychiatric disorders.

References

Abe Y, Sakai Y, Nishida S, Nakamae T, Yamada K, Fukui K, Narumoto J (2015) Hyper-influence of the orbitofrontal cortex over the ventral striatum in obsessive-compulsive disorder. Eur Neuropsychopharm 25:1898–1905.

Autio JA, Glasser MF, Ose T, Donahue CJ, Bastiani M, Ohno M, Kawabata Y, Urushibata Y, Murata K, Nishigori K, Yamaguchi M, Hori Y, Yoshida A, Go Y, Coalson TS, Jbabdi S, Sotiropoulos SN, Kennedy H, Smith S, Van Essen DC, Hayashi T (2020) Towards HCP-style macaque connectomes: 24-channel 3T multi-array coil, MRI sequences and preprocessing. Neuroimage 215:116800.

Baxter MG, Parker A, Lindner CCC, Izquierdo AD, Murray EA (2000) Control of response selection by reinforcer value requires interaction of amygdala and orbital prefrontal cortex. J Neurosci 20:4311–4319.

Baxter MG, Gaffan D, Kyriazis DA, Mitchell AS (2009) Ventrolateral prefrontal cortex is required for performance of a strategy implementation task but not reinforcer devaluation effects in rhesus monkeys. Eur J Neurosci 29:2049–2059.

Berridge KC (2004) Motivation concepts in behavioral neuroscience. Physiol Behav 81:179–209.

Bouret S, Richmond BJ (2010) Ventromedial and orbital prefrontal neurons differentially encode internally and externally driven motivational values in monkeys. J Neurosci 30:8591–8601.

Chaudhry AM, Parkinson JA, Hinton EC, Owen AM, Roberts AC (2009) Preference judgements involve a network of structures within frontal, cingulate and insula cortices. Eur J Neurosci 29:1047–1055.

Clark AM, Bouret S, Young AM, Murray EA, Richmond BJ (2013) Interaction between orbital prefrontal and rhinal cortex is required for normal estimates of expected value. J Neurosci 33:1833–1845.

Critchley HD, Rolls ET (1996) Olfactory neuronal responses in the primate orbitofrontal cortex: analysis in an olfactory discrimination task. J Neurophysiol 75:1659–1672.

de Araujo IE, Rolls ET (2004) Representation in the human brain of food texture and oral fat. J Neurosci 24:3086–3093.

Dickinson A, Balleine BW (1994) Motivational control of goal-directed action. Animal Learning and Behavior 22:1–18.

Donahue CJ, Sotiropoulos SN, Jbabdi S, Hernandez-Fernandez M, Behrens TE, Dyrby TB, Coalson T, Kennedy H, Knoblauch K, Essen DCV, Glasser MF (2016) Using diffusion tractography to predict cortical connection strength and distance: a quantitative comparison with tracers in the monkey. J Neurosci 36:6758–6770.

Donahue CJ, Glasser MF, Preuss TM, Rilling JK, Essen DCV (2018) Quantitative assessment of prefrontal cortex in humans relative to nonhuman primates. Proc Natl Acad Sci U S A 115:E5183–E5192.

Eldridge MAG, Lerchner W, Saunders RC, Kaneko H, Krausz KW, Gonzalez FJ, Ji B, Higuchi M, Minamimoto T, Richmond BJ (2016) Chemogenetic disconnection of monkey orbitofrontal and rhinal cortex reversibly disrupts reward value. Nat Neurosci 19:37–39.

Fettes P, Schulze L, Downar J (2017) Cortico-striatal-thalamic loop circuits of the orbitofrontal cortex: promising therapeutic targets in psychiatric illness. Front Syst Neurosci 11:25.

Figee M, Luigjes J, Smolders R, Valencia-Alfonso CE, van Wingen G, de Kwaasteniet B, Mantione M, Ooms P, de Koning P, Vulink N, Levar N, Droge L, van den Munckhof P, Schuurman PR, Nederveen A, van den Brink W, Mazaheri A, Vink M, Denys D (2013) Deep brain stimulation restores frontostriatal network activity in obsessive-compulsive disorder. Nat Neurosci 16:386–387.

Foerde K, Steinglass J, Shohamy D, Walsh BT (2015) Neural mechanisms supporting maladaptive food choices in anorexia nervosa. Nat Neurosci 18:1571–1573.

Fujimoto A, Hori Y, Nagai Y, Kikuchi E, Oyama K, Suhara T, Minamimoto T (2019) Signaling incentive and drive in the primate ventral pallidum for motivational control of goal-directed action. J Neurosci 39:1793–1804.

Gillan CM, Robbins TW (2014) Goal-directed learning and obsessive–compulsive disorder. Phil Trans R Soc B Biol Sci 369:20130475.

Gillan CM, Papmeyer M, Morein-Zamir S, Sahakian BJ, Fineberg NA, Robbins TW, de Wit S (2011) Disruption in the balance between goal-directed behavior and habit learning in obsessive-compulsive disorder. Am J Psychiatry 168:718–726.

Gillan CM, Kosinski M, Whelan R, Phelps EA, Daw ND (2016) Characterizing a psychiatric symptom dimension related to deficits in goal-directed control. Elife 5:e11305.

Gremel CM, Costa RM (2013) Orbitofrontal and striatal circuits dynamically encode the shift between goal-directed and habitual actions. Nat Commun 4:2264–2264.

Gremel CM, Chancey JH, Atwood BK, Luo G, Neve R, Ramakrishnan C, Deisseroth K, Lovinger DM, Costa RM (2016) Endocannabinoid modulation of orbitostriatal circuits gates habit formation. Neuron 90:1312–1324.

Griffiths KR, Morris RW, Balleine BW (2014) Translational studies of goal-directed action as a framework for classifying deficits across psychiatric disorders. Front Syst Neurosci 8:101.

Haber SN, Kim K-S, Mailly P, Calzavara R (2006) Reward-related cortical inputs define a large striatal region in primates that interface with associative cortical connections, providing a substrate for incentive-based learning. J Neurosci 26:8368–8376.

Harrison BJ, Soriano-Mas C, Pujol J, Ortiz H, López-Solà M, Hernández-Ribas R, Deus J, Alonso P, Yücel M, Pantelis C, Menchon JM, Cardoner N (2009) Altered corticostriatal functional connectivity in obsessive-compulsive disorder. Arch Gen Psychiatry 66:1189–1200.

Hirabayashi T, Nagai Y, Hori Y, Inoue K, Aoki I, Takada M, Suhara T, Higuchi M, Minamimoto T (2021) Chemogenetic sensory fMRI reveals behaviorally relevant bidirectional changes in primate somatosensory network. Neuron 109:3312–3322.e5.

Hollerman JR, Tremblay L, Schultz W (1998) Influence of reward expectation on behavior-related neuronal activity in primate striatum. J Neurophysiol 80:947–963.

Hosokawa T, Kennerley SW, Sloan J, Wallis JD (2013) Single-neuron mechanisms underlying cost-benefit analysis in frontal cortex. J Neurosci 33:17385–17397.

Izquierdo A, Suda RK, Murray EA (2004) Bilateral orbital prefrontal cortex lesions in rhesus monkeys disrupt choices guided by both reward value and reward contingency. J Neurosci 24:7540–7548.

Jahanshahi M, Obeso I, Rothwell JC, Obeso JA (2015) A fronto-striato-subthalamic-pallidal network for goal-directed and habitual inhibition. Nat Rev Neurosci 16:719–732.

Kobayashi S, Carvalho OP, de Schultz W (2010) Adaptation of reward sensitivity in orbitofrontal neurons. J Neurosci 30:534–544.

Machado CJ, Bachevalier J (2007) The effects of selective amygdala, orbital frontal cortex or hippocampal formation lesions on reward assessment in nonhuman primates. Eur J Neurosci 25:2885–2904.

McFarland NR, Haber SN (2002) Thalamic relay nuclei of the basal ganglia form both reciprocal and nonreciprocal cortical connections, linking multiple frontal cortical areas. J Neurosci 22:8117–8132.

Minamimoto T, Camera GL, Richmond BJ (2009) Measuring and modeling the interaction among reward size, delay to reward, and satiation level on motivation in monkeys. J Neurophysiol 101:437–447.

Minamimoto T, Yamada H, Hori Y, Suhara T (2012) Hydration level is an internal variable for computing motivation to obtain water rewards in monkeys. Exp Brain Res 218:609–618.

Mitchell AS, Browning PGF, Baxter MG (2007) Neurotoxic lesions of the medial mediodorsal nucleus of the thalamus disrupt reinforcer devaluation effects in rhesus monkeys. J Neurosci 27:11289–11295.

Murray EA, Moylan EJ, Saleem KS, Basile BM, Turchi J (2015) Specialized areas for value updating and goal selection in the primate orbitofrontal cortex. Elife 4:e11695.

Nagai Y, Kikuchi E, Lerchner W, Inoue KI, Ji B, Eldridge MA, Kaneko H, Kimura Y, Oh-Nishi A, Hori Y, Kato Y, Hirabayashi T, Fujimoto A, Kumata K, Zhang MR, Aoki I, Suhara T, Higuchi M, Takada M, Richmond BJ, Minamimoto T (2016) PET imaging-guided chemogenetic silencing reveals a critical role of primate rostromedial caudate in reward evaluation. Nat Commun 7:13605.

Nagai Y, et al. (2020) Deschloroclozapine, a potent and selective chemogenetic actuator enables rapid neuronal and behavioral modulations in mice and monkeys. Nat Neurosci 23:1157–1167.

Nakamura K, Santos GS, Matsuzaki R, Nakahara H (2012) Differential reward coding in the subdivisions of the primate caudate during an oculomotor task. J Neurosci 32:15963–15982.

Ng TH, Alloy LB, Smith DV (2019) Meta-analysis of reward processing in major depressive disorder reveals distinct abnormalities within the reward circuit. Transl Psychiat 9:293.

Oguchi M, Tanaka S, Pan X, Kikusui T, Moriya-Ito K, Kato S, Kobayashi K, Sakagami M (2021) Chemogenetic inactivation reveals the inhibitory control function of the prefronto-striatal pathway in the macaque brain. Commun Biol 4:1088.

Oyama K, Hori Y, Nagai Y, Miyakawa N, Mimura K, Hirabayashi T, Inoue K, Suhara T, Takada M, Higuchi M, Minamimoto T (2021) Chemogenetic dissection of the primate prefronto-subcortical pathways for working memory and decision-making. Sci Adv 7:eabg4246.

Padoa-Schioppa C, Assad JA (2006) Neurons in the orbitofrontal cortex encode economic value. Nature 441:223–226.

Pastor-Bernier A, Stasiak A, Schultz W (2021) Reward-specific satiety affects subjective value signals in orbitofrontal cortex during multicomponent economic choice. Proc National Acad Sci U S A 118:e2022650118.

Rich EL, Wallis JD (2016) Decoding subjective decisions from orbitofrontal cortex. Nat Neurosci 19:973–980.

Roesch MR, Olson CR (2004) Neuronal activity related to reward value and motivation in primate frontal cortex. Science 304:307–310.

Rolls ET, Sienkiewicz ZJ, Yaxley S (1989) Hunger modulates the responses to gustatory stimuli of single neurons in the caudolateral orbitofrontal cortex of the macaque monkey. Eur J Neurosci 1:53–60.

Rudebeck PH, Saunders RC, Prescott AT, Chau LS, Murray EA (2013a) Prefrontal mechanisms of behavioral flexibility, emotion regulation and value updating. Nat Neurosci 16:1140–1145.

Rudebeck PH, Mitz AR, Chacko RV, Murray EA (2013b) Effects of amygdala lesions on reward-value coding in orbital and medial prefrontal cortex. Neuron 80:1519–1531.

Russchen FT, Amaral DG, Price JL (1987) The afferent input to the magnocellular division of the mediodorsal thalamic nucleus in the monkey, *Macaca fascicularis*. J Comp Neurol 256:175–210.

Sha Z, Versace A, Edmiston EK, Fournier J, Graur S, Greenberg T, Santos JPL, Chase HW, Stiffler RS, Bonar L, Hudak R, Yendiki A, Greenberg BD, Rasmussen S, Liu H, Quirk G, Haber S, Phillips ML (2020) Functional disruption in prefrontal-striatal network in obsessive-compulsive disorder. Psychiatry Res Neuroimaging 300:111081.

Simmons JM, Minamimoto T, Murray EA, Richmond BJ (2010) Selective ablations reveal that orbital and lateral prefrontal cortex play different roles in estimating predicted reward value. J Neurosci 30:15878–15887.

Smith SM, Jenkinson M, Woolrich MW, Beckmann CF, Behrens TEJ, Johansen-Berg H, Bannister PR, Luca MD, Drobnjak I, Flitney DE, Niazy RK, Saunders J, Vickers J, Zhang Y, Stefano ND, Brady JM, Matthews PM (2004) Advances in functional and structural MR image analysis and implementation as FSL. Neuroimage 23:S208–S219.

Voon V, Derbyshire K, Rück C, Irvine MA, Worbe Y, Enander J, Schreiber LRN, Gillan C, Fineberg NA, Sahakian BJ, Robbins TW, Harrison NA, Wood J, Daw ND, Dayan P, Grant JE, Bullmore ET (2015) Disorders of compulsivity: a common bias towards learning habits. Mol Psychiatry 20:345–352.

West EA, DesJardin JT, Gale K, Malkova L (2011) Transient inactivation of orbitofrontal cortex blocks reinforcer devaluation in macaques. J Neurosci 31:15128–15135.

Xiao D, Zikopoulos B, Barbas H (2009) Laminar and modular organization of prefrontal projections to multiple thalamic nuclei. Neuroscience 161:1067–1081.

Yan X, Telu S, Dick RM, Liow J-S, Zanotti-Fregonara P, Morse CL, Manly LS, Gladding RL, Shrestha S, Lerchner W, Nagai Y, Minamimoto T, Zoghbi SS, Innis RB, Pike VW, Richmond BJ, Eldridge MA (2021) [11C] deschloroclozapine is an improved PET radioligand for quantifying a human muscarinic DREADD expressed in monkey brain. J Cereb Blood Flow Metab 41:2571–2582.

Yin HH, Ostlund SB, Knowlton BJ, Balleine BW (2005) The role of the dorsomedial striatum in instrumental conditioning. Eur J Neurosci 22:513–523.

Yun M, Kawai T, Nejime M, Yamada H, Matsumoto M (2020) Signal dynamics of midbrain dopamine neurons during economic decision-making in monkeys. Sci Adv 6:eaba4962.

Zhang J, Berridge KC, Tindell AJ, Smith KS, Aldridge JW (2009) A neural computational model of incentive salience. Plos Comput Biol 5:e1000437.